J. Fluid Mech. (1998), *vol.* 361, *pp.* 1–24. Printed in the United Kingdom

Conditional scalar dissipation statistics in a turbulent counterflow

By KATERINA SARDI, A. M. K. P. TAYLOR AND J. H. WHITELAW

Mechanical Engineering Department, Imperial College of Science, Technology and Medicine, Exhibition Road, London SW7 2BX, UK

(Received 28 November 1996 and in revised form 13 November 1997)

Cold-wire measurements of a scalar, temperature, its fluctuations and the axial and radial components of the scalar dissipation between two opposed turbulent jet flows, where one jet was slightly heated, show that the residence times of the scalar in the mixing layer were short, that the scalar fluctuations and their dissipation were strongly correlated and that the probability distributions of the conditional scalar dissipation components were log-normal at values of the dissipation larger than the mean. The first finding is consistent with the fact that the scalar turbulence was 'young', in the sense that residence times were shorter than the large-eddy turn-over time, so that the results are likely to be representative of scalar turbulence when scalar mixing first takes place between two streams, for example close to the stabilization region of turbulent diffusion flames. The second implies that the mean scalar dissipation, conditional on the stoichiometric mixture fraction, is larger than the unconditional mean by up to an order of magnitude. Dependence of the distributions of the mean and r.m.s. conditional scalar dissipation on the shape of the scalar p.d.f. was demonstrated by relating the largest conditional dissipation values to the rarest scalar fluctuations and it was found that this dependence was also valid in other flows where scalar dissipation has been measured. The third finding implies that the use of a log-normal distribution to describe the p.d.f. of the conditional scalar dissipation, in the context of flame extinction modelling, will be in error by only 15% provided that the mean and the r.m.s. conditional scalar dissipation are accurately known.

1. Introduction

The measurements presented here are relevant to the representation of passive scalar mixing when it first takes place between two streams and comprise distributions of temperature, its fluctuations and their dissipation in the mixing layer between two opposed jet flows with one at a slightly higher temperature. The statistical properties of a passive scalar, its fluctuations and their dissipation at early stages of mixing between two streams are interesting from a fundamental point of view. Our study has been motivated by the particular example of combustion in turbulent diffusion flames where the joint probability distribution of the fuel mixture fraction and the scalar dissipation and the mean scalar dissipation conditional on the stoichiometric mixture fraction are proportional to the mean reaction rate (Bilger 1980). Furthermore, local extinction of diffusion flames is postulated to occur where the conditional scalar dissipation exceeds a critical quenching value (Peters 1983; Bilger 1988), and global extinction is considered to take place when the cumulative probability of the values

of the conditional dissipation, larger than the quenching value, exceeds a critical threshold (Liew, Bray & Moss 1984; Lee & Pope 1995).

In the context of combustion and extinction calculations, based on time-averaged equations of the unconditional scalar dissipation, the probability distribution of the conditional scalar dissipation and its mean value must be known or modelled. A convenient practice (Janicka & Peters 1982; Liew *et al.* 1984; Haworth, Drake & Blint 1988), is to consider that the mean conditional scalar dissipation is equal to the mean unconditional value, by assuming that the mixture fraction and the dissipation of its fluctuations are statistically independent, that is their joint p.d.f. is equal to the product of the two individual p.d.f.s, and to assume that the probability density function of the conditional scalar dissipation is log-normally distributed. The merits of these two representations, suggested by Bilger (1980) and Kolmogorov (1962) respectively, must be decided by recourse to experiment but available measurements of the scalar field of diffusion flames and, in particular, of the mixture fraction dissipation, its statistics and joint statistics are limited because of the requirements for advanced optical techniques, so the validity of the modelling approximations has not been thoroughly assessed. The measurements that do exist tend to suggest that the assumption of statistical independence between mixture fraction and scalar dissipation is not valid near the air–flame boundary and that the probability distribution of the unconditional dissipation deviates from log-normality, possibly because of intermittency (Stårner *et al.* 1994; Everest *et al.* 1995).

Structural information about the scalar field and its dissipation can also be acquired by measuring a passive scalar in non-combusting flows. This approach has the advantage that measurements can be performed using the cold-wire method which is better documented than optical techniques. Even though there are several publications that report measurements of a scalar and its dissipation, the assumption of independence was examined only in few cases. These include the studies of Anselmet & Antonia (1985), Jayesh & Warhaft (1992), Kailasnath, Sreenivasan & Saylor (1993) and Anselmet, Djeridi & Fulachier (1994) in round and square jets, wakes and boundary layers who found that a correlation between the passive scalar and the dissipation existed when the scalar fluctuations were large. The statistical distributions of the unconditional and conditional scalar dissipation were examined by Sreenivasan, Antonia & Dahn (1977) and Namazian, Scheffer & Kelly (1988) in a boundary layer and a round jet respectively who concluded, as did Everest *et al.* (1995) in a combusting flow, that the individual components of the unconditional scalar dissipation deviated from log-normality due to intermittency effects but argued that the overall dissipation distribution can be adequately described as log-normal. However, the majority of the existing publications (Tavoularis & Corrsin 1980; Antonia & Browne 1986; Krishnamoorthy & Antonia 1987; Antonia & Mi 1993), focus on the mean values of the scalar dissipation and on the anisotropy between the components rather than on the statistical distributions. Nevertheless, there seems to be no theoretical connection between the departures from local isotropy and flame extinction although Mi, Antonia & Anselmet (1995) have argued that when the statistical independence between mixture fraction and scalar dissipation is not justified, the temperature fluctuations are strongly asymmetrical and local isotropy does not exist.

Our aim is to extend knowledge to configurations relevant to the first stages of turbulent mixing between two streams. In this context, the primary purpose of the present work is to provide new evidence on the statistical relationship between the scalar fluctuations and their dissipation and on the probability distributions of the conditional dissipation in a flow representative of the stabilization region of diffusion

flames and thus to quantify the implications in the modelling of turbulent diffusion flame extinction. The scalar field within the mixing layer created by opposed jet flows has been selected because it offers the advantage of short residence times, in comparison to the eddy turn-over time, simulating the conditions present in the stabilization region of practical flames and has the merits of the simplicity of the flow field and the uniformity of the strain rate (Bray, Champion & Libby 1994).

The measurements presented in this paper include the single and joint probability distributions of the scalar fluctuations and the axial and radial components of their dissipation along the centreline between two opposing jets. The results are reported in terms of a normalized temperature which has the properties of a mixture fraction. The assumption of log-normality is assessed for the unconditional and the conditional scalar dissipation and the origin and magnitude of the correlation between the scalar and its dissipation is quantified. The values of the mean and r.m.s. conditional scalar dissipation were evaluated as a function of this mixture fraction so as to provide a complete mapping of the conditional dissipation statistics. We identify a dependence between the distributions of the mean and r.m.s. conditional scalar dissipation and the shape of the scalar p.d.f. and which is found to be valid in other flows where scalar dissipation has been measured.

2. Experimental arrangement and instrumentation

The flow configuration is shown in figure 1 and is similar to that considered by Mastorakos, Taylor & Whitelaw (1993). It comprised two identical vertically-opposed contoured nozzles with a contraction area ratio of 9 over a 90 mm contraction length followed by a 50 mm straight section of 30 mm diameter. The nozzles were separated by a distance, H, equal to one nozzle diameter and perforated plates with solidity of 45% and 4 mm hole diameter were located immediately upstream of the straight section of each nozzle. The passive scalar was introduced by heating the upper stream to 25°C above ambient, with a tolerance of ± 1°C, using an electric heater (Hotwatt 9128, 4.8 kW). The flow to the upper nozzle was thermally insulated and both jets were shielded from ambient disturbances by surrounding annular air flows.

In order to quantify the effect of the Reynolds number on the evolution of the conditional scalar dissipation, measurements were obtained with two velocities different by 40%. In one case, the bulk velocity, U_b, of the cold jet was 3.84 m s^{-1} and that of the heated jet was 4 m s^{-1} so that the momenta of the two jets were equal and the stagnation plane was located at the half distance, $H/2$, between the two opposing jets. The Reynolds number based on the nozzle diameter at the exit plane was of the order of 7500, the bulk strain rate, $S_b = 2U_b/H$, was 260 s^{-1} and the residence time in the mixing layer, $t_{RES} = 1/S_b$, was about 3.8 ms. For the other case, the velocities of the cold and the heated jets were 5.44 m s^{-1} and 5.7 m s^{-1} respectively, the corresponding Reynolds number was 10 480 and the bulk strain rate achieved the value of 376 s^{-1} so that the residence time in the mixing layer was about 2.6 ms.

The radial profiles of the mean and r.m.s. of the axial velocity component at the exit plane of the two jets, measured with a tungsten hot-wire probe (DANTEC 55P11) connected to a bridge (DISA 55M10) operating at an overheat ratio of 1.8, are presented in figure 2. It can be seen that the mean velocity profiles were flat for more than 45% of the nozzle radius, R, and that the normalized r.m.s. of the axial turbulent fluctuations, u'/U_b, was 0.1 and independent of bulk velocity. The integral length scale, L_t, at the jet exit planes was considered equal to 70% of the hole diameter of the perforated plate, as has been measured by Cho *et al.* (1988) and

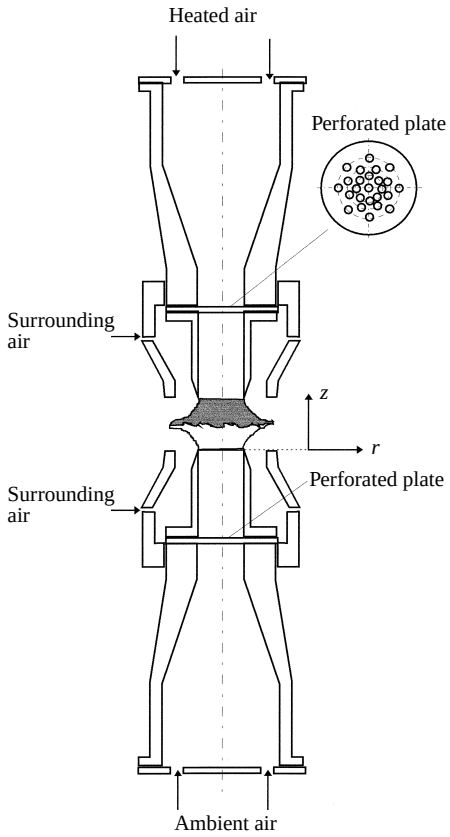

FIGURE 1. The counterflow arrangement.

Kostiuk (1991). The turbulent Reynolds numbers, R_t, based on the integral length scale and the axial velocity fluctuations were 73 and 102, the large-eddy turn-over time, $t_{ov} = L_t/u'$, achieved the values of 7.2 ms and 5.1 ms and the Kolmogorov microscale was estimated to be of the order of 0.13 mm and 0.1 mm for the lower and the 40% higher velocities respectively. Note that the turbulent Reynolds numbers were evaluated at the exit planes of the opposed jets and would increase towards stagnation by a factor of about two, as shown experimentally by Kostiuk, Bray & Cheng (1989) and Mastorakos, Taylor & Whitelaw (1992) and theoretically by Champion & Libby (1990) and Bray, Champion & Libby (1991).

Parallel cold wires (AUSPEX, Pennsylvania, USA, Dantec Compatible, A55P71) and a custom-built constant-current circuit were used to measure temperature characteristics including the instantaneous temperature, T, presented below in terms of a mixture fraction $\Theta = (T - T_c)/(T_h - T_c)$, where T_c and T_h are the temperatures of the cold and hot jets at their exit planes respectively, the normalized temperature fluctuations, θ, from the mean scalar value and the axial and radial components of their dissipation, $\chi_z = 2D_t(\partial\theta/\partial x_z)^2$ and $\chi_r = 2D_t(\partial\theta/\partial x_r)^2$ where D_t is the air thermal diffusivity assumed constant and equal to 2.2 10^{-5} $m^2\,s^{-1}$, and z and r are the axial and radial coordinates shown in figure 1. Simultaneous measurements of temperature fluctuations and the axial and radial components of the scalar dissipation were obtained with pairs of parallel, fully etched, platinum wires with prongs tapered to a tip diameter of 75 μm and sensors 0.5 μm in diameter and 0.6 mm long for the axial

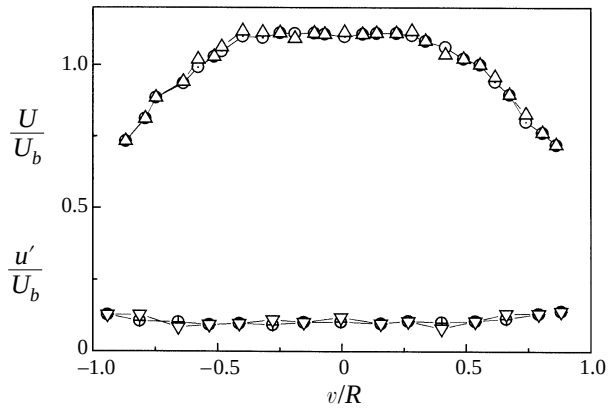

FIGURE 2. Mean axial velocities and r.m.s. axial fluctuations, normalized with the bulk velocity, at the exit of the lower and the upper jets: ○, mean velocity of the lower jet; ⊕, r.m.s. velocity of the lower jet; △, mean velocity of the upper jet; ▽, r.m.s. velocity of the lower jet.

component and 0.4 mm for the radial, resulting in a maximum length to diameter ratio, l_w/d_w, of 1200, and in a wire length to Kolmogorov length scale ratio, l_w/n_k, of 4.6. The uncertainty in the measurements, due to end conduction effects and the influence of the thermal boundary layer created on the prongs, was estimated to be of the order of 15% (Parathoen, Petit & Lecordier 1982; Tsuji, Nagano & Tagawa 1993), while the spatial attenuation was of the order of 20% (Wyngaard 1971*a*). The separation between the two parallel sensors was fixed at 0.3 mm and was selected (Sardi 1997), after measuring the axial squared gradient of the temperature fluctuations at each point along the centreline by parallel probes of spacing in the range of 0.2–0.4 mm according to the procedure proposed by Anselmet *et al.* (1994). The time constant of the sensors in the vicinity of the stagnation plane, evaluated from the relation proposed by Collis & Williams (1959), was 20 μs resulting in a cut-off frequency of 8 kHz and thus approximately a factor of two higher than the estimated Kolmogorov frequency of 4.7 kHz and so no compensation was required.

The constant-current circuit comprised two, nominally identical, electronic circuits, one for each sensor of the twin probe. In each circuit, a constant-voltage power supply drove a constant-current chip providing 0.1 mA constant to ± 0.5 μA, so that the velocity sensitivity of the sensors was of the order of 1% (Wyngaard 1971*b*). The signal was amplified and offset to increase the resolution and was interfaced to a Personal Computer (INTEL 486, 33 MHz) by a 16-bit A/D card (ANALOGIC HSDAS). The sampling rate was 8 kHz and 2^{16} samples were obtained at each point along the centreline so as to ensure statistical convergence for the unconditional and the conditional values of the scalar dissipation.

3. Results and discussion

This section presents measurements of the single and joint scalar–scalar dissipation statistical distributions along the centreline of the counterflow, and the sequence of presentation begins with the single-point probability distributions in §3.1 before progressing to the arguably more important joint distributions in §3.2. Since the main objective of this work is to provide information on the joint probability distributions of the scalar and its dissipation and on the conditional statistics of the scalar dissipation within the mixing layer, the averaged values of the mean and r.m.s. distributions of

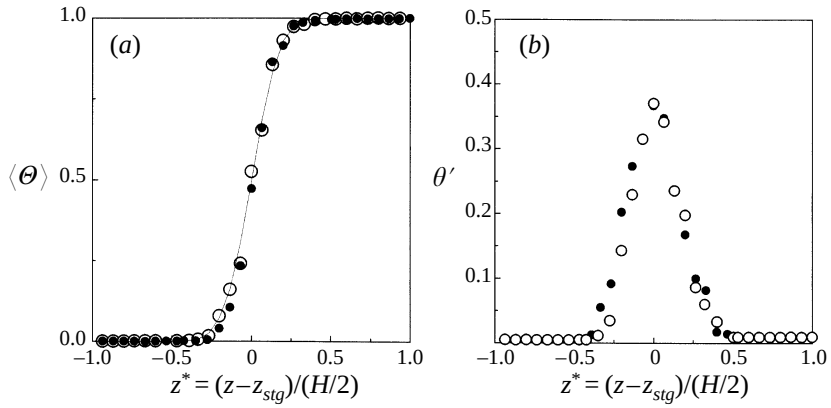

FIGURE 3. (*a*) Mean and (*b*) r.m.s. scalar distributions along the centreline as a function of Reynolds number: filled symbols $Re = 7500$; open symbols $Re = 10480$.

the scalar and of the unconditional dissipation are outlined only briefly in the next paragraph and the reader is referred to Sardi, Taylor & Whitelaw (1996) for a more detailed discussion of these quantities.

The measurements revealed that the mean normalized temperature, $\langle\Theta\rangle$, along the centreline between the two jets can be approximated by an error function, with zero and unity at the cold and hot boundaries and 0.5 at the stagnation plane where the r.m.s. of the scalar fluctuations, θ', achieved its maximum value, as shown in figure 3 in which the axial distance along the centreline has been normalized as $z^* = (z - z_{stg})/(H/2)$ and $z_{stg} = H/2$ is the location of the stagnation plane. It is clear that the distributions of the mean scalar and its fluctuations, and hence the mean thickness of the mixing layer between the hot and the cold streams, were independent of bulk velocity for the two Reynolds numbers examined, as has been also shown by Mastorakos *et al.* (1993). The axial and radial mean and r.m.s. scalar dissipation components, normalized by half the bulk strain rate $S_b/2 = U_c/H$, also achieved their maximum values at the stagnation plane and decreased towards the exits of the opposed jets, as shown in figure 4. The normalized distributions are similar for the two bulk velocities, implying a proportional increase of the scalar dissipation with Reynolds number in agreement with the direct numerical simulations of Ashurst *et al.* (1987). The ratios of the mean and r.m.s. of the axial to the radial components, $\langle\chi_z\rangle/\langle\chi_r\rangle$ and χ_z'/χ_r', were approximately equal to 4 at the stagnation point, for both Reynolds numbers, implying that local isotropy was not satisfied in the mixing layer created by two opposed jets as has been also found in wind tunnel turbulence (Sreenivasan & Tavoularis 1980; Tavoularis & Corrsin 1981), plane jets (Antonia & Van Atta 1975; Antonia & Sreenivasan 1977; Anselmet & Antonia 1985), wakes (Antonia & Browne 1986; Prasad & Sreenivasan 1990) and boundary layers (Sreenivasan *et al.* 1977; Kailasnath *et al.* 1993) for turbulent Reynolds numbers based on the Taylor microscale as high as 240.

3.1. *Probability distributions of scalar fluctuations and scalar dissipation*

This section presents the scalar p.d.f.s along the centreline together with the associated distributions of the axial and radial components of the scalar dissipation: the former is to demonstrate that this scalar field is characterized by an unusually broad range of probability distributions and to identify the boundaries of the mixing layer, and the latter is to assess the applicability of the assumption of log-normality.

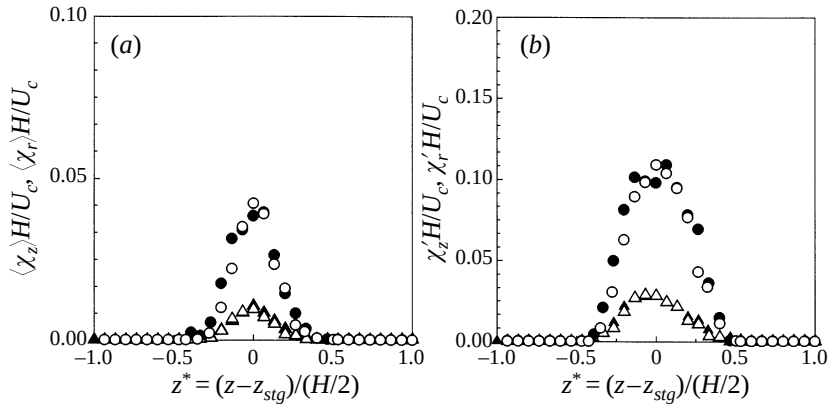

FIGURE 4. Mean (*a*) and (*b*) r.m.s. distributions of the axial and radial components of the scalar dissipation along the centreline as a function of Reynolds number; filled symbols $Re = 7500$; open symbols $Re = 10480$; circles, axial component; triangles, radial component.

$z^\star$	$\langle\Theta\rangle$	θ'
−0.6	0.000 45	0.000 43
−0.46	0.000 6	0.006
−0.26	0.019	0.095
−0.13	0.184	0.28
0.0	0.54	0.37

TABLE 1. Values of normalizing variables of figures 5, 11, 12 and 13.

The p.d.f.s of the scalar fluctuations normalized by their respective r.m.s values, see table 1, are shown in figure 5 at selected locations along the centreline for a bulk velocity of the cold jet of 3.84 ms^{-1}, and in figure 6 the skewness, $K_3 = \langle\theta^3\rangle/\langle\theta^2\rangle^{3/2}$, of the scalar fluctuations along the centreline is presented for both bulk velocities to show that the evolution of the scalar p.d.f.s is similar for the two Reynolds numbers over most of the mixing layer. At the edges of the mixing layer† $z^* = -0.26$, mixing takes place due to the rare events of hot high-amplitude fluctuations which cross the mean stagnation plane and cause skewness of the p.d.f. of scalar fluctuations of up to 20, figure 6. Near the stagnation plane, on the colder side of the mixing layer, $z^* = -0.13$, the probability of fluctuations from the hotter side increases and the skewness is reduced by a factor of two while the probability distribution is symmetrical ($K_3 = 0$) and bimodal at the stagnation plane, suggesting that sharp transitions of equal probability take place between the cold and the hot fluid. The spatial evolution of the p.d.f.s is symmetrical with respect to the stagnation plane and, thus, at positive values of z^* the scalar evolves with the values of the highest probability being those corresponding to the hotter fluid.

The bimodality of the scalar probability distribution at the stagnation plane is consistent with the fact that the residence time in the mixing layer was too short for

† The p.d.f.s in figure 5(*a*) and 5(*j*), at $z^\star = -0.6$ and 0.6, correspond to almost unmixed fluid with low r.m.s. scalar fluctuation, θ', of 0.0044 (table 1); thus the quasi-Gaussian distribution plotted is, primarily, due to electronic noise, amplified by the normalization procedure. At $z^\star = -0.46$, figure 5(*b*), the mean scalar concentration has increased and the p.d.f. changes to a narrower Gaussian distribution with a noticeable lack of tails.

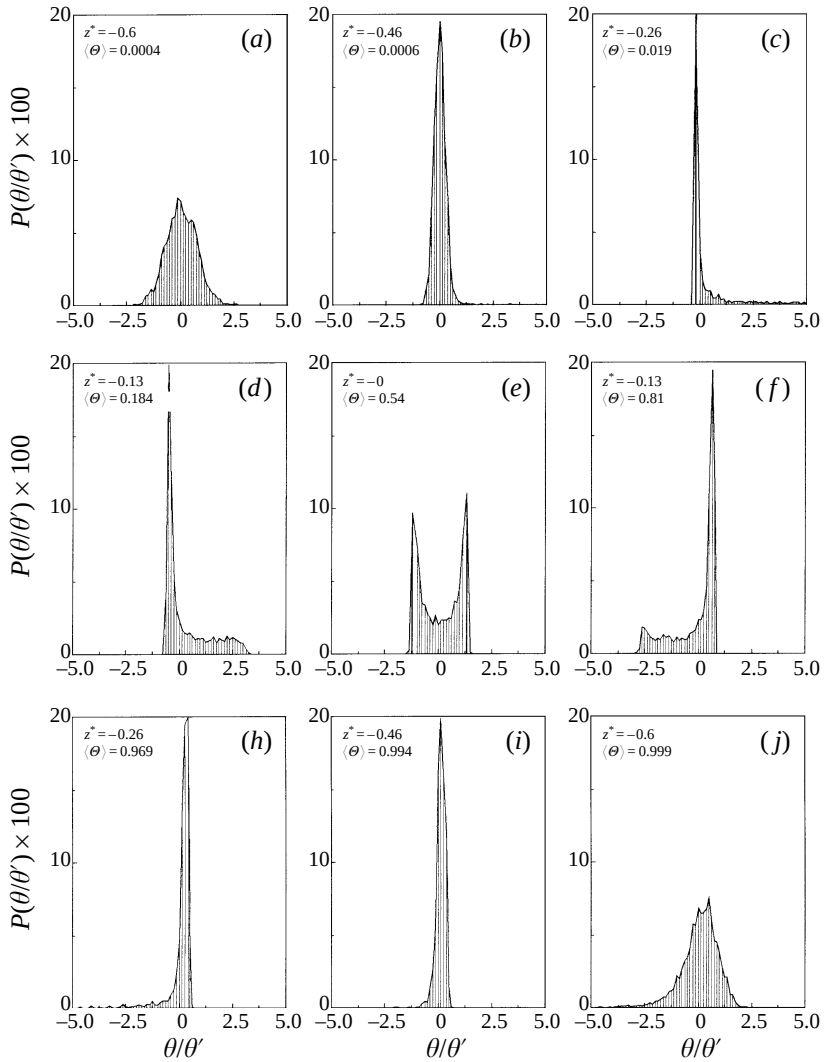

FIGURE 5. Probability distributions of the scalar fluctuations along the centreline between the two jets ($Re = 7500$).

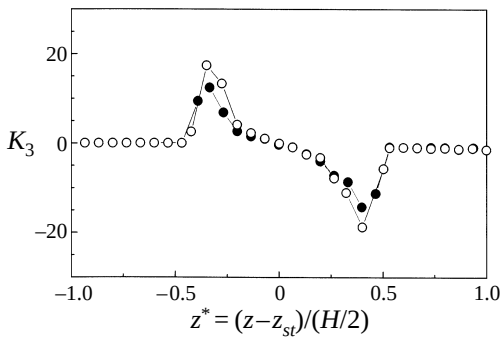

FIGURE 6. Skewness of the scalar fluctuations along the centreline: filled symbols $Re = 7500$; open symbols $Re = 10\,480$.

	$\langle\chi_z\rangle$ (s^{-1})		χ_z' (s^{-1})	
$z^\star$	$Re = 7500$	$Re = 10\,480$	$Re = 7500$	$Re = 10\,480$
−0.6	0.02	0.02	0.03	0.03
−0.46	0.13	0.20	0.29	0.47
−0.26	0.18	0.39	6.27	6.54
−0.13	2.24	4.00	13.06	16.17
0.0	4.90	7.70	12.61	19.80

TABLE 2. Values of normalizing variables of figures 7, 9 and 11–15.

	$\langle\chi_r\rangle$ (s^{-1})		χ_r' (s^{-1})	
$z^\star$	$Re = 7500$	Re=10 480	Re=7500	Re=10 480
−0.6	0.02	0.04	0.03	0.03
−0.46	0.05	0.11	0.06	0.11
−0.26	0.22	0.24	0.83	1.18
−0.13	0.80	1.26	2.71	3.34
0.0	1.36	1.82	3.68	5.30

TABLE 3. Values of normalizing variables of figure 8.

the growth of large-scale wrinkles at the scalar interface and thus the instantaneous temperature profile in the axial direction increased monotonically from zero to unity. Bimodality of the scalar p.d.f. has also been encountered behind a line scalar source decaying into wind-tunnel turbulence, (Stapountzis *et al.* 1986), and in direct numerical simulations (Eswaran & Pope 1988), and is evidence that the turbulent scalar field was 'young' in the sense that the residence time of the scalar within the interface was shorter than that required for one eddy turn-over.

The probability distributions of the axial and radial components of the unconditional scalar dissipation for the two bulk velocities are multiplied by the local mean values, $\langle\chi_z\rangle$ and $\langle\chi_r\rangle$, (see tables 2 and 3) and plotted in semi-logarithmic coordinates in figures 7 and 8, for the cold half of the centreline only; the hot half was the same within experimental accuracy. It can be seen that the region of highest probability corresponds to values of the normalized dissipation lower than unity while long exponential-like tails of low probability extend to dissipation values as high as 15 times the mean. The p.d.f.s of the axial and the radial components of the scalar dissipation are similar and evolve with the same trend for the two Reynolds numbers with small differences due to the 0.5 mm uncertainty in the repeatability of position of the traversing mechanism.

The cumulative distribution, c.d.f., of the total unconditional scalar dissipation is

$$\text{c.d.f.}\,(\chi) = \int_0^{\chi} P(\chi^*)\mathrm{d}\chi^* \tag{3.1}$$

where χ^* is a dummy variable and represents, in the context of flame extinction calculations, the probability that a flame burns (Liew *et al.* 1984). In order to assess whether the distribution is indeed log-normal, the cumulative distributions of the natural logarithms of the unconditional, χ_z, and the conditional axial component of the scalar dissipation, $\chi_z|\Theta_{st}$, where Θ_{st} is an arbitrary value of the instantaneous scalar, are plotted in figure 9 in probability coordinates for a Reynolds number of 10 480; the cumulative distributions of the radial components are bound to be similar

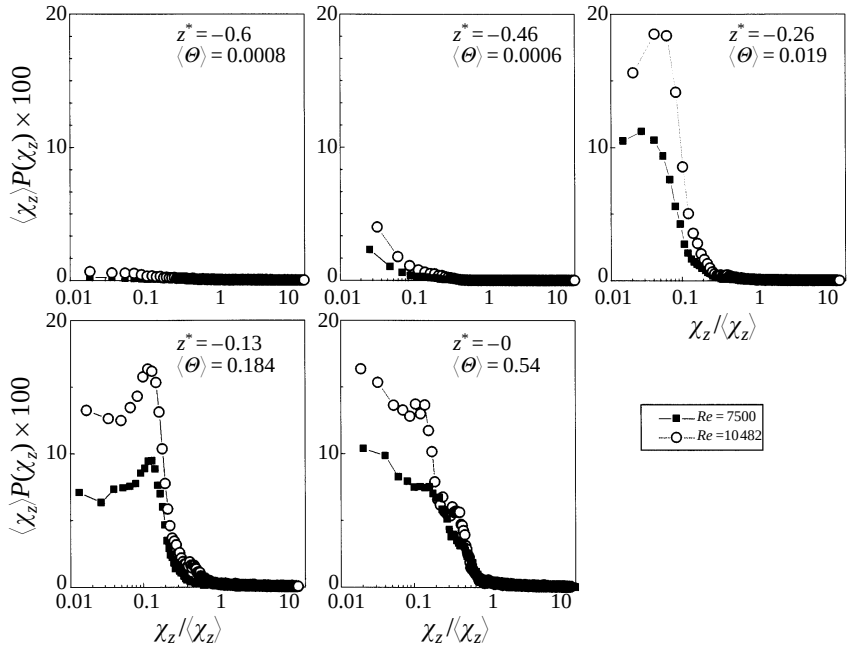

FIGURE 7. Probability distributions of the axial component of the scalar dissipation, plotted for semi-logarithmic axes, at five stations along the 'cold' half of the centreline.

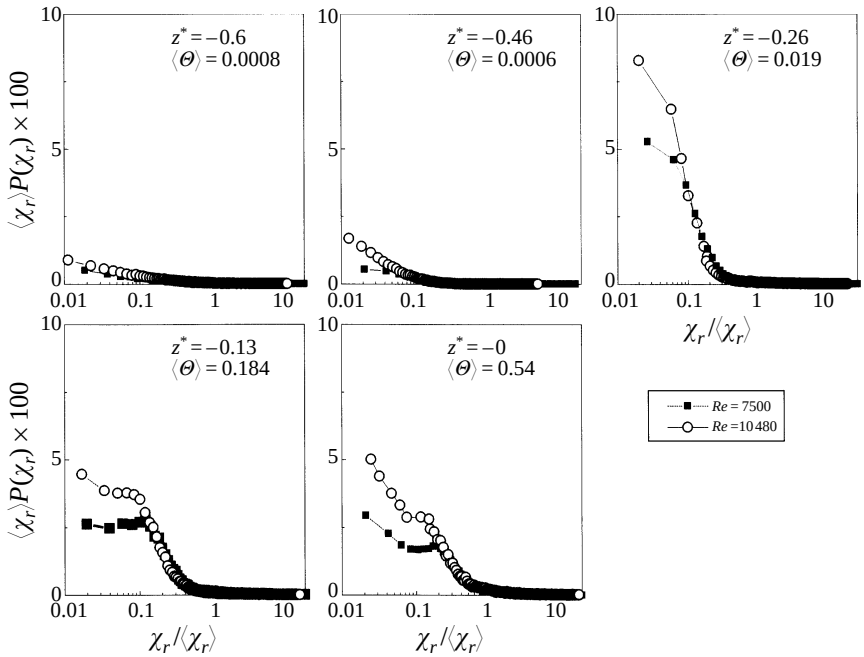

FIGURE 8. Probability distributions of the radial component of the scalar dissipation, plotted for semi-logarithmic axes, at five stations along the 'cold' half of the centreline.

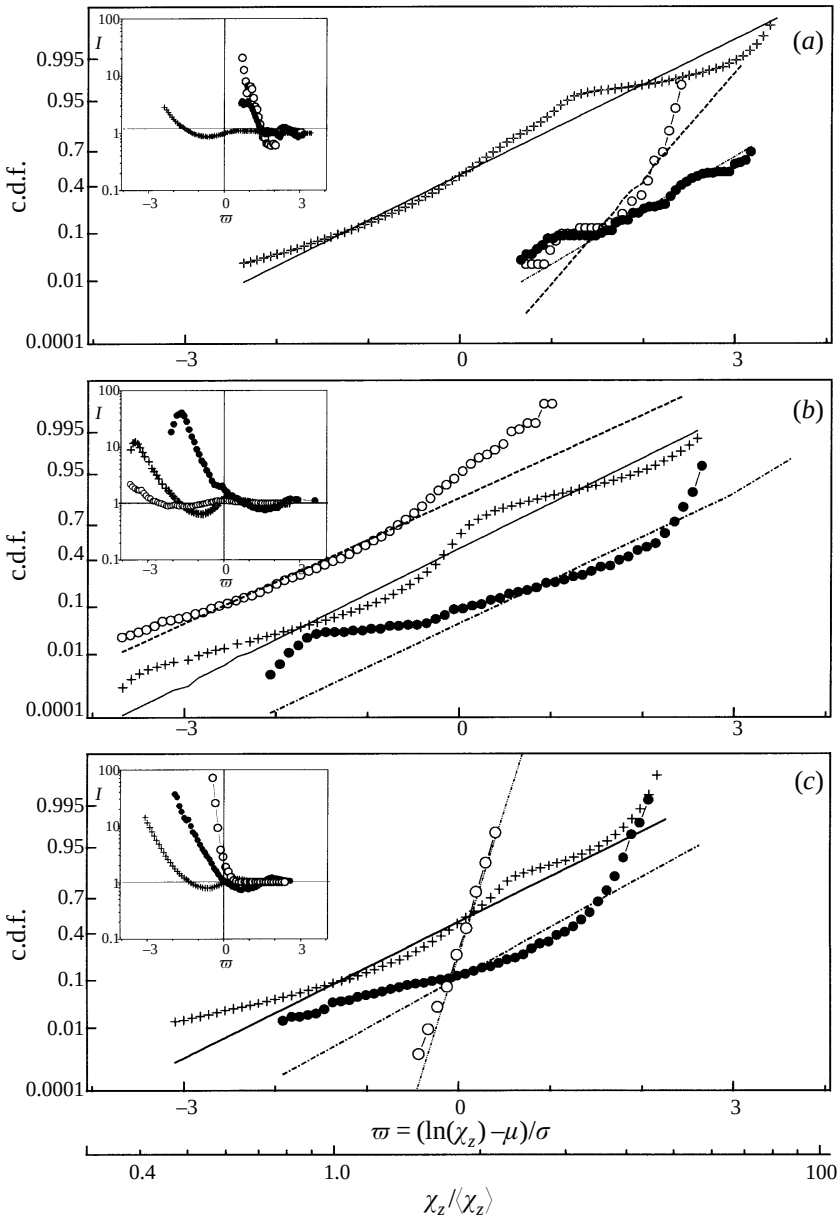

FIGURE 9. Cumulative probability distributions of the unconditional and conditional scalar dissipation at three locations along the centreline: (*a*) $z^\star = -0.27$ (*b*), $z^\star = -0.13$ and (*c*) $z^\star = 0$. The deviation indices from log-normality are shown as inserted graphs at the left-hand side of all plots: +++, unconditional; -○-, conditional at $\Theta_{st} = 0.055$; -●-, conditional at $\Theta_{st} = 0.3$; ——, unconditional log-normal; — — — log-normal conditional at $\Theta_{st} = 0.055$; ·····, log-normal conditional at $\Theta_{st} = 0.3$.

since their p.d.f.s evolved with the same trends as those of the axial components of figure 7 as shown in figure 8. The conditional values have been chosen to correspond to instantaneous scalar concentrations, Θ_{st}, of 0.055 and 0.3 which represent the stoichiometric mixture fractions of methane and CO/H_2 flames in air with a CO/H_2 molar ratio equal to 0.6. The respective cumulative probabilities based on an assumed

log-normal distribution are also shown and were evaluated by integrating the following expressions:

$$P(\ln(\chi_z)) = \frac{1}{\sigma_z(2\pi)^{1/2}} \exp\left[-\frac{(\ln(\chi_z) - \mu_z)^2}{2\sigma_z^2}\right], \tag{3.2}$$

$$P(\ln(\chi_z|\Theta_{st})) = \frac{1}{\sigma_{z_{st}}(2\pi)^{1/2}} \exp\left[-\frac{(\ln(\chi_z|\Theta_{st}) - \mu_{z_{st}})^2}{2\sigma_{z_{st}}^2}\right]. \tag{3.3}$$

Here the pairs of constants μ_z and σ_z and $\mu_{z_{st}}$ and $\sigma_{z_{st}}$ are the mean and r.m.s. of the natural logarithm of the measured samples of the unconditional and conditional axial component of the scalar dissipation respectively, calculated from

$$\mu_z = \frac{1}{N}\sum_{i=1}^{N} \ln(\chi_z)_i, \quad \sigma_z^2 = \left(\frac{1}{N}\sum_{i=1}^{N} \ln(\chi_z)_i\right)^2 - \mu_z^2, \tag{3.4}$$

$$\mu_{z_{st}} = \frac{1}{N_{st}}\sum_{i=1}^{N_{st}} \ln(\chi_{z_{st}})_i, \quad \sigma_{z_{st}}^2 = \left(\frac{1}{N_{st}}\sum_{i=1}^{N_{st}} \ln(\chi_{z_{st}})_i\right)^2 - \mu_{z_{st}}^2, \tag{3.5}$$

where subscript i represents an individual measurement, N is the total number of samples and N_{st} is the number of the measured dissipation samples which correspond to values of the scalar equal to the stoichiometric value, Θ_{st}, within a bin width of $\pm 5\%$ of Θ_{st}. At the high dissipation values, the selection of a single component to assess the assumption of log-normality for the probability distribution of the total dissipation can be justified from the previous work of Sreenivasan *et al.* (1977) and Prasad & Sreenivasan (1990) who showed, by measuring simultaneously all three components in jets, boundary layers and wakes, that the statistical distribution of an individual component can provide a surrogate for the total scalar dissipation p.d.f. At the low values of the scalar dissipation, the measurements of Sreenivasan *et al.* (1977) revealed that departures from log-normality, due to intermittency, are amplified if the individual components, rather than the total unconditional scalar dissipation, are plotted. In this context, differences between the c.d.f. of the axial component and the log-normal distribution, equations (3.2)–(3.5), identified in the remainder of this section, are presented to provide an estimate of the maximum possible deviation of the total unconditional or conditional distributions from log-normality.

If a random variable is log-normally distributed then by definition the cumulative probability of its natural logarithm is linear when plotted in probability coordinates (Kerstein & Ashurst 1984). From figure 9 it can be seen that departures from log-normality exist both for the unconditional and the conditional c.d.f.s and that conditional c.d.f.s tend to deviate more from log-normality than the respective unconditional distributions. The deviation has been quantified by the values of the deviation indices, I, defined by Namazian *et al.* (1988),

$$I(\chi_z) = \frac{\text{c.d.f.}\,(\ln(\chi_z))}{\displaystyle\int_{-\infty}^{\ln(\chi_z)} \frac{1}{(2\pi)^{1/2}} e^{-\varpi^2} d\varpi}, \tag{3.6a}$$

$$I(\chi_z|\Theta_{st}) = \frac{\text{c.d.f.}\,(\ln(\chi_z|\Theta_{st}))}{\displaystyle\int_{-\infty}^{\ln(\chi_z|\Theta_{st})} \frac{1}{(2\pi)^{1/2}} e^{-\varpi_{st}^2} d\varpi_{st}}, \tag{3.6b}$$

and plotted in the inserted graphs of figure 9. The indices collapse to unity for log-normally distributed dependent variables. In equations (3.6), ϖ and ϖ_{st} are the standardized variables of a normal distribution,

$$\varpi = \frac{\ln(\chi_z) - \mu_z}{\sigma_z} \quad \text{and} \quad \varpi_{st} = \frac{\ln(\chi_{st_z}) - \mu_{st_z}}{\sigma_{st_z}}, \tag{3.7}$$

depending on whether the unconditional or the conditional scalar dissipation distributions are examined.

It can be seen that, for values of ϖ lower than approximately unity, the deviation indices are of the order of 10 for the c.d.f. of the unconditional dissipation but achieve values as high as 80 for the conditional distributions. However it should be noted that *for values of ϖ greater than unity* the deviation index tends to one, suggesting that the low-probability, exponential tails of both unconditional and conditional distributions are, to a good approximation, log-normal. This is important because the critical value of the cumulative probability below which burning cannot be sustained, estimated from percolation theory, is of the order of 68–75% (Peters 1984), and it can be seen from figure 9 that this always corresponds to values of ϖ greater than unity. Hence, the adoption of log-normality – even for the distribution of one component of the conditional scalar dissipation in a 'young' turbulent flow such as the mixing layer created between the opposed jets – is likely to lead to prediction of extinction limits to within 15%.

Note, however, in figure 9 that the unconditional and conditional cumulative distributions do not coincide but, on the contrary, are greatly displaced from each other. This implies, as shown and quantified in the next section, that an error in the estimation of the quenching probability occurs if the values of the mean, μ, and r.m.s., σ, of the natural logarithm of the unconditional scalar dissipation are used as input parameters in the evaluation of the log-normal c.d.f., instead of the respective conditional values, μ_{st} and σ_{st}.

3.2. *Statistical dependence of scalar dissipation on scalar fluctuations*

This section quantifies the departures from statistical independence both by evaluating the correlation coefficient, $\rho_{\theta,\chi}$, of the scalar fluctuations and their dissipation and by comparing the joint probability distribution $P(\theta, \chi)$ with the product of the individual p.d.f.s $P(\theta)P(\chi)$. The former approach provides a rapid overview which confirms that it is not sensible to use the unconditional dissipation instead of the conditional value, while the latter includes complete information on the joint scalar statistics which is useful for evaluations of models for the joint p.d.f. From the point of view of identifying *the origin* of the correlation between the scalar and its dissipation, however, the complex joint distributions are not helpful and thus the analysis proceeds through the presentation of weighted joint p.d.f.s which reveal that successful models of joint and conditional statistics must be able to predict the value of the scalar fluctuations at which the large values of dissipation occur. It is reasonable to expect that this is a formidable modelling challenge and, thus, it is relevant to inquire as to the likely magnitude of the error involved if statistical independence is assumed, and this is addressed and quantified in §3.3. It will be argued that the current findings concerning the conditional values of the scalar dissipation depend on, and are determined by, the probability distribution of the scalar p.d.f. and, although obtained for a counterflow geometry, the conclusions are applicable to the stabilization region of many practical combustors.

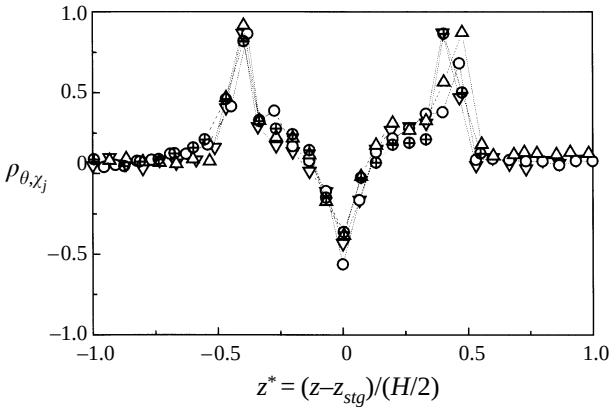

FIGURE 10. Distribution of the correlation coefficient between the scalar fluctuations and the scalar dissipation, along the centreline; ○, ρ_{θ,χ_z}, $Re = 7500$; ⊕, ρ_{θ,χ_z}, $Re = 10\,480$; △, ρ_{θ,χ_r}, $Re = 7500$; ▽, ρ_{θ,χ_r}, $Re = 10\,480$.

Figure 10 shows the correlation coefficient between the scalar fluctuations and the axial and radial components of the scalar dissipation

$$\rho_{\theta,\chi_j} = \frac{\left\langle \left(\Theta^2 - \langle\Theta^2\rangle\right)\left(\chi_j - \langle\chi_j\rangle\right)\right\rangle}{\left\langle \left(\Theta^2 - \langle\Theta^2\rangle\right)^2\right\rangle^{1/2}\left\langle \left(\chi_i - \langle\chi_i\rangle\right)^2\right\rangle^{1/2}} \tag{3.8}$$

for the two Reynolds numbers. For non-zero values of the correlation coefficient, the scalar fluctuations and the scalar dissipation are statistically related but if the correlation coefficient is equal to zero they are not necessarily statistically independent (Tennekes & Lumley 1972), and further investigation by comparing the joint p.d.f. to the product of the individual p.d.f.s is required in order to assess the dependence of the scalar dissipation on the scalar fluctuations. It can be seen that the correlation coefficient is almost zero outside the mixing layer, achieves a maximum value of unity at the edges of the interface both for the axial and for the radial components – which implies that the scalar fluctuations and their dissipation are perfectly correlated – and decreases to approximately −0.5 at the stagnation plane independent of Reynolds number. Gao (1991) showed that in a homogeneous scalar field the scalar fluctuation and the scalar dissipation are statistically independent if and only if the scalar p.d.f. has a Gaussian distribution. This finding is also applicable to the current non-homogeneous scalar field established by the mixing layer between the opposed jets. It can be seen, figure 10, that the correlation coefficient is not zero and the scalar p.d.f. is not Gaussian within the mixing layer, figure 5. Anselmet *et al.* (1994) and Mi *et al.* (1995) related the dependence of the scalar dissipation on the scalar fluctuations to the asymmetry of the scalar p.d.f. by observing that the two variables are independent when the skewness of the scalar fluctuations is zero, which is clearly the case when the scalar p.d.f. is Gaussian. However this cannot be so when the scalar fluctuations are symmetrical and their probability distribution is not Gaussian, as demonstrated by the bimodal p.d.f. of zero skewness at the stagnation plane of the counterflow, figure 6, which results in a value of −0.5 for the correlation coefficient.

If the assumption of independence between Θ and χ_j were valid then, by definition, the joint probability distribution of the scalar fluctuations and their dissipation, $P(\theta, \chi_j)$, would be equal to the product of the individual p.d.f.s, $P(\theta)P(\chi_j)$. Since it

was shown in figure 10 that the distributions of the correlation coefficient along the centreline between the opposed jets are similar for the axial and the radial components only the joint p.d.f.s $P(\theta, \chi_z)$ and $P(\theta)P(\chi_z)$ are shown in figure 11. The joint p.d.f.s are presented at five stations along the cold half of the centreline for a Reynolds number of 10 480, in terms of the centred normalized scalar fluctuations, θ^+, and scalar dissipation, χ_z^+.

$$\theta^+ = \frac{\Theta - \langle \Theta \rangle}{\theta'} \quad \text{and} \quad \chi_z^+ = \frac{\chi_z - \langle \chi_z \rangle}{\langle \chi_z \rangle} \tag{3.9}$$

and were evaluated over a mesh of 100×100 bins in the range $[-5, 5]$ and $[-2, 16]$ of centred scalar fluctuations and scalar dissipation and all normalizing quantities are summarized in tables 1 and 2.

At $z^\star = -0.6$, figure 11(*a*), outside the main part of the mixing layer, the correlation coefficient is zero and the joint p.d.f., $P(\theta, \chi_z)$, is similar to the product of the individual distributions, $P(\theta)P(\chi_j)$, so that the scalar and its dissipation are uncorrelated and statistically independent since the corresponding scalar p.d.f. is Gaussian, figure 3(*a*). Within the mixing layer, $-0.6 < z^\star < 0.6$, figure 11(*b–e*), the products of the individual p.d.f.s tend to underpredict the probability of occurrence of the higher values of the dissipation. Close to the stagnation plane, at $z^\star = -0.13$, the joint p.d.f. displays the bimodal features of the flow field but the result of the assumption of statistical independence does not. At the stagnation plane, figure 11(*e*), the product of the individual p.d.f.s of the scalar fluctuations and the scalar dissipation successfully reproduces the bimodality of the scalar field but again tends to underestimate the probability of occurrence of values of dissipation larger than the mean, i.e. for $\chi_z^+ > 0$.

The correlation coefficient and the comparison of the joint p.d.f.s with the product of the individual p.d.f.s identifies the locations at which the statistical independence hypothesis breaks down and illustrates some of the consequences of its use on the prediction of flame extinction. This is useful information but is limited in that it does not provide guidance for identification of the physical processes that give rise to the correlation between the scalar fluctuations and their dissipation. The contribution of each part of the scalar fluctuations and scalar dissipation space to their overall correlation can be examined in terms of a weighting function integrand (Anselmet *et al.* 1994), defined as

$$W_{\theta,\chi_z} = \theta^+ \chi_z^+ P(\theta^+, \chi_z^+) \tag{3.10}$$

so that the double integral of $\theta^+ \chi_z^+ P(\theta^+, \chi_z^+)$ over scalar fluctuation and dissipation space is the correlation coefficient ρ_{θ,χ_z}. Figure 12 shows the weighting integrands, $\theta^+ \chi_z^+ P(\theta^+, \chi_z^+)$, for the locations of figure 11 while the quantity $\theta^+ \chi_z^+ P(\theta^+)P(\chi_z^+)$ is also plotted for comparison, so that when the two terms are identical the correlation coefficient is zero, figure 12(*a*).

The correlation at the boundaries of the mixing layer, figure 12(*b–d*), is caused by the large and positive scalar fluctuations, associated with the exponential tails of the scalar p.d.f., figure 5, which give rise to values of instantaneous dissipation 10 to 15 times higher than the mean. Figure 12(*e*) corresponds to the stagnation plane where the bimodal features of the scalar field are adequately described by the statistical independence assumption, as discussed in connection with figure 11(*e*), but the largest instantaneous dissipation values are related to small scalar fluctuation and not to the positive fluctuations, as predicted by the weighting integrand $\theta^+ \chi_z^+ P(\theta^+)P(\chi_z^+)$. The dependence of the values of the scalar dissipation on the scalar fluctuations provides further evidence that the scalar field is 'young', in the sense that the cascade process

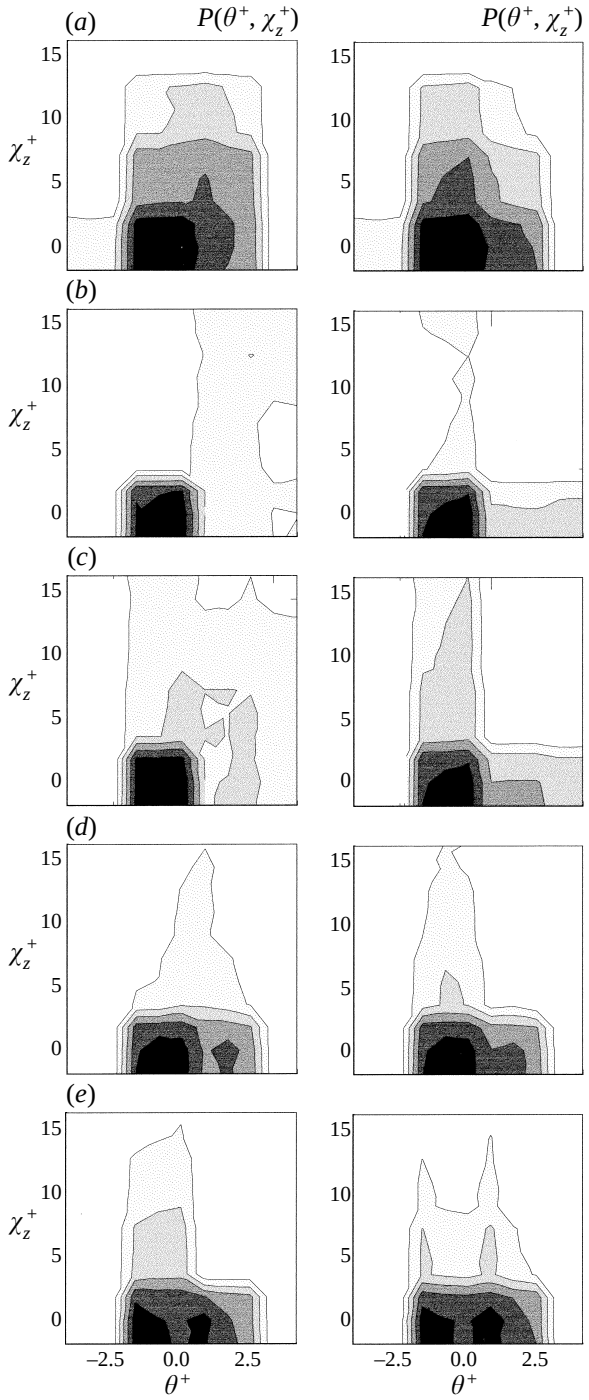

FIGURE 11. Joint probability distributions of the scalar fluctuations and the axial component of their dissipation. The graphs in the left-hand column present the joint p.d.f., $P(\theta^+, \chi_z^+)$, and the graphs in the right-hand column show the product of the individual p.d.f.s, $P(\theta^+)P(\chi_z^+)$, at five axial locations: (*a*) $z^\star = -0.6$, (*b*) $z^\star = -0.46$, (*c*) $z^\star = -0.26$, (*d*) $z^\star = -0.13$, (*e*) $z^\star = 0$. In all figures contour lines are drawn, from inner to outer, at 0.35, 0.13, 0.05, 0.019, 0.007, 0.003.

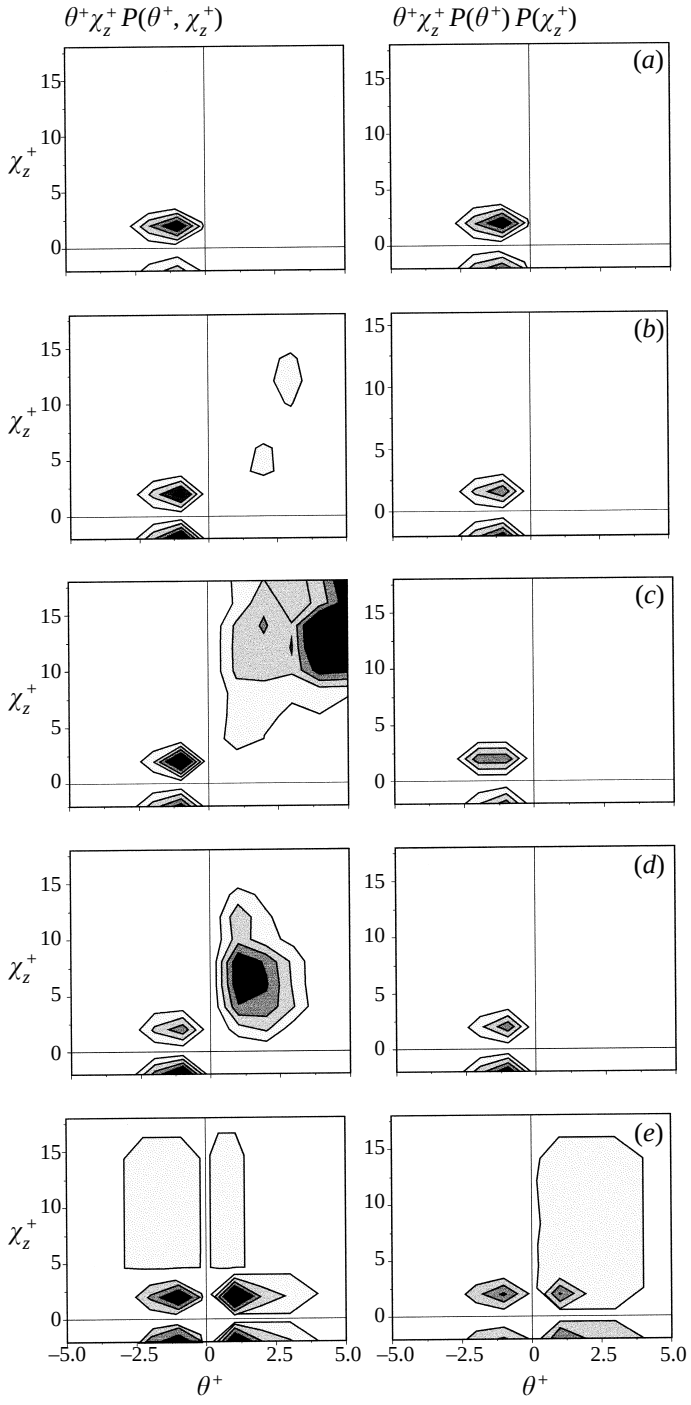

FIGURE 12. Iso-contours of the weighting functions of the scalar fluctuations and the axial component of their dissipation. The left-hand column presents the weighting integrands $\theta^+\chi_z^+ P(\theta^+, \chi_z^+)$ and the right-hand column shows the term $\theta^+\chi_z^+ P(\theta^+)P(\chi_z^+)$, at the locations of figure 11. In (*a–d*) contour lines are drawn, from inner to outer, at 0.08, 0.064, 0.048, 0.032, 0.016. In (*e*), contour lines are drawn at 0.08, 0.06, 0.04, 0.02 for negative values of θ^+ and $\chi_z^+ < 5$ and at −0.08, −0.06, −0.04, −0.02 for positive values of θ^+ or $\chi_z^+ \geqslant 5$.

has no time to propagate down to the smallest scales due to the short residence times in the mixing layer, so that the smallest turbulent scales depend on the large scales, and this is further supported by the lack of local isotropy of the scalar dissipation in the axial and radial direction along the centreline of the opposed jets.

3.3. *Conditional distributions*

Successful modelling of conditional scalar statistics, for example in the context of combustion calculations, depends on knowledge of three parameters: the mean scalar dissipation conditional on the stoichiometric mixture fraction, $\langle\chi|\Theta_{st}\rangle$, the weighted probability, $E_{\chi|\Theta_{st}}$, of occurrence of the mean conditional scalar dissipation and the r.m.s. conditional dissipation, $\chi'|\Theta_{st}$, defined respectively as

$$\langle\chi|\Theta_{st}\rangle \equiv \int_0^\infty \chi P(\chi|\Theta_{st})\mathrm{d}\chi = \frac{1}{N_{st}}\sum_{i=1}^{N_{st}}(\chi|\Theta_{st})_i, \tag{3.11}$$

$$E_{\chi|\Theta} \equiv \langle\chi|\Theta_{st}\rangle P(\Theta = \Theta_{st}), \tag{3.12}$$

$$\chi'|\Theta_{st} \equiv \left(\int_0^\infty (\chi - \langle\chi|\Theta_{st}\rangle)^2 P(\chi|\Theta_{st})\mathrm{d}\chi\right)^{1/2} = \left(\frac{1}{N_{st}}\sum_{i=1}^{N_{st}}\left(\chi|\Theta_{st} - \langle\chi|\Theta_{st}\rangle\right)_i^2\right)^{1/2}, \tag{3.13}$$

where N_{st} is the number of scalar dissipation samples corresponding to the stoichiometric mixture fraction.

The distributions of the mean and r.m.s. of the conditional dissipation, equations (3.11) and (3.13), are related to the parameters μ_{st} and σ_{st} of the log-normal distribution, equation (3.3), for the conditional scalar dissipation by

$$\langle\chi|\Theta_{st}\rangle = \mathrm{e}^{(\mu_{st}+\sigma/2)}, \tag{3.14}$$

$$\chi'|\Theta_{st} = \left(\langle\chi|\Theta_{st}\rangle^2 \mathrm{e}^{(\sigma_{st}^2-1)}\right)^{1/2}. \tag{3.15}$$

The term $E_{\chi|\Theta_{st}}$ in equation (3.12), estimated via (3.11), represents the molecular diffusion in scalar space in the transport equation for the scalar p.d.f. (Sahay & O' Brien 1993), and is also proportional to the mean reaction rate (Bilger 1980).

Figure 13 presents the distributions of the mean and r.m.s. of the axial scalar dissipation component conditional on the scalar fluctuations and of the weighted probability $E_{\chi|\Theta_{st}}$, equation (3.12), all normalized by the mean unconditional scalar dissipation value $\langle\chi_z\rangle$ so that if the scalar dissipation is independent of the scalar fluctuations $\langle\chi_z|\Theta_{st}\rangle/\langle\chi_z\rangle = 1$ and $E_{\chi|\Theta_{st}}$ coincides with the scalar p.d.f., $P(\theta)$. All conditional statistics have been calculated for the same mesh size and the same range of scalar fluctuations and dissipation, equation (3.9), used in the evaluation of the joint p.d.f.s. The statistical uncertainty, $\Sigma^N = ((\chi_z'|\theta)^2/N_{st})^{1/2}$, in the values of the mean conditional scalar dissipation was estimated to be less than 5% (Girimmett & Stirzaker 1992). Far from the mixing layer, at $z^\star = -0.6$, figure 13(*a*), where the assumption of independence is valid, the distributions of mean and r.m.s. conditional dissipation are indeed close to straight lines, parallel to the horizontal scalar fluctuation axis, over large extents of centred scalar fluctuations θ^+, and the normalized probability is almost Gaussian. At the boundaries of the mixing layer, $z^\star = -0.46$ and $z^\star = -0.26$, the largest values of mean conditional scalar dissipation, which can be 50 times the unconditional mean, correspond to the largest positive values of the

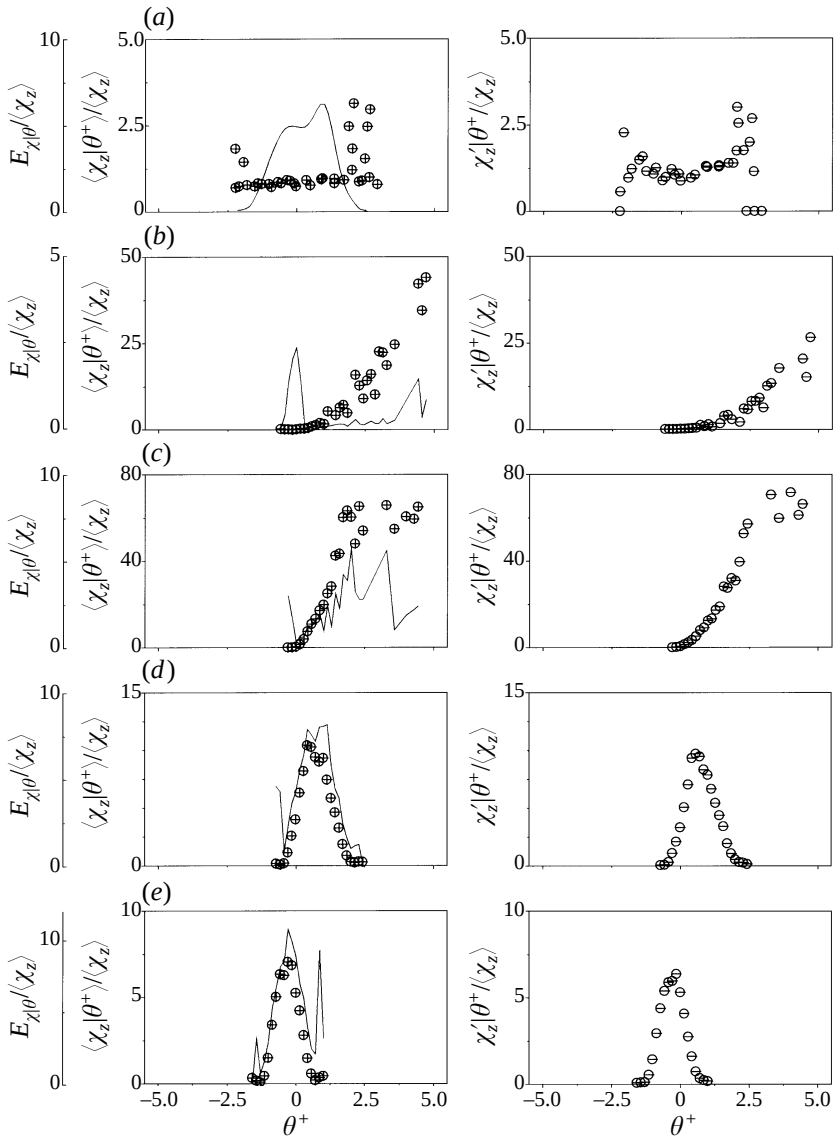

FIGURE 13. Mean and r.m.s of the axial component of the scalar dissipation conditional on the scalar fluctuations and the probability of occurrence of the former at the locations of figure 11: ⊕, mean conditional dissipation; ⊖, r.m.s. conditional dissipation; ——, weighted probability $E_{\chi|\theta}$.

scalar fluctuations and the distribution has the shape of a half-parabola, for $\theta \geqslant 0$. At $z^\star = -0.13$, however, the distribution changes to an inverted shape, which is retained at the stagnation plane where the largest conditional dissipation corresponds to small values of scalar fluctuations.

Comparison of figure 13 with the p.d.f.s of the scalar fluctuations, figure 5, shows that the largest values of the mean conditional dissipation correspond always to the rarest values of scalar fluctuations, which are located at the tail end of the p.d.f. at the edges of the mixing layer, and between the two peaks of the bimodal distribution at $z^\star = 0$. This pairing of the rare scalar fluctuations with the high values of mean

conditional scalar dissipation can be also identified in other flow configurations, for example in the grid turbulence of Jayesh & Warhaft (1992) in which the scalar p.d.f. was ∩-shaped with high probability of zero scalar fluctuations and tails at positive and negative values, and the distribution of the mean conditional dissipation had a ∪-shape with the largest mean dissipation, $\langle\chi|\theta\rangle$, at the rare large positive and negative fluctuations. Anselmet *et al.* (1994) examined the scalar field in the mixing layer of a jet and reported a skewed scalar p.d.f. with the high-probability region at negative fluctuations and a low-probability exponential-like tail at positive fluctuations. The resulting distribution for the mean conditional scalar dissipation, $\langle\chi|\theta\rangle$, included low values at the most probable negative scalar fluctuations and the maximum value of $\langle\chi|\theta\rangle$ at the largest, rarest, positive values of scalar fluctuations. Thus, in all reported flows where statistical independence was not satisfied, and this is likely to be true when the scalar p.d.f. is not Gaussian, the distribution of the mean conditional dissipation is directly related to, and can be qualitatively described by, the scalar p.d.f. which relates low scalar probability to conditional dissipation values higher than the unconditional mean and high probability to conditional values lower than the unconditional mean. This implies that in combustion calculations, where a functional form of the scalar p.d.f. is often assumed, a qualitative description of the mean conditional dissipation can be obtained in terms of the inverse of the scalar p.d.f.

The r.m.s. of the conditional scalar dissipation, $\chi_z'|\theta$, is almost equal to, and is similarly distributed to, the mean conditional dissipation so that the maximum values of $\chi_z'|\theta$ also correspond to the rarest scalar fluctuations. Although the absence of published data of the r.m.s. conditional dissipation from other flow configurations prevents comments on the generality of this result, the p.d.f. of the scalar dissipation, where it has been measured (Sreenivasan *et al.* 1977; Namazian *et al.* 1988), was always characterized by a high probability region at small values of dissipation and long exponential tails and thus resembled an exponential distribution where, by definition, the mean is equal to the r.m.s value. This result is important for the modelling of the standard deviation of the cumulative distribution of the scalar dissipation via the log-normality assumption, particularly since even the unconditional r.m.s. scalar dissipation cannot be evaluated directly from a second-moment closure or a transport p.d.f. equation.

The implications for combustion calculations and predictions of flame extinction depend on the value of the stoichiometric mixture fraction and will be discussed in terms of the scalar values $\Theta_{st} = 0.055$ and 0.3 corresponding to methane and air and CO/H_2 and air diffusion flames, the latter of CO/H_2 molar ratio of 0.6. Figures 14(*a*) and 15(*a*) present the distributions of the mean, $\langle\chi_z|\Theta_{st}\rangle$, and r.m.s., $\chi_z'|\Theta_{st}$, conditional scalar dissipation normalized by their respective unconditional values, $\langle\chi_z\rangle$ and χ_z', and plotted as a function of the mean scalar concentration, $\langle\Theta\rangle$, along the centreline between the two jets. Figures 14(*b*) and 15(*b*) show the distributions of the weighted probability $E_{\chi|\Theta_{st}}$, equation (3.13), and the scalar probability $P(\Theta_{st})$, of occurrence of the values of 0.055 and 0.3 respectively. It can be seen that the ratios $\langle\chi_z|\Theta_{st}\rangle/\langle\chi_z\rangle$ and $\chi_z'|\Theta_{st}/\chi_z'$ decrease from the boundaries to the centre of the mixing layer for both scalar values, Θ_{st}, and the mean and r.m.s. of the scalar dissipation conditional on $\Theta_{st} = 0.055$ are lower than the unconditional values while $\langle\chi_z|\Theta_{st}\rangle/\langle\chi_z\rangle$ and $\chi_z'|\Theta_{st}/\chi_z'$ conditional on $\Theta_{st} = 0.3$ are larger than unity within the mixing layer. At the maximum values of the scalar probability, $P(\Theta_{st})$, figures 14(*b*) and 15(*b*), which correspond to the *most probable locations* for the stabilization of a turbulent diffusion flame, the mean and r.m.s. of the conditional dissipation can differ by at least an order of magnitude from the respective unconditional values. This implies that calculations

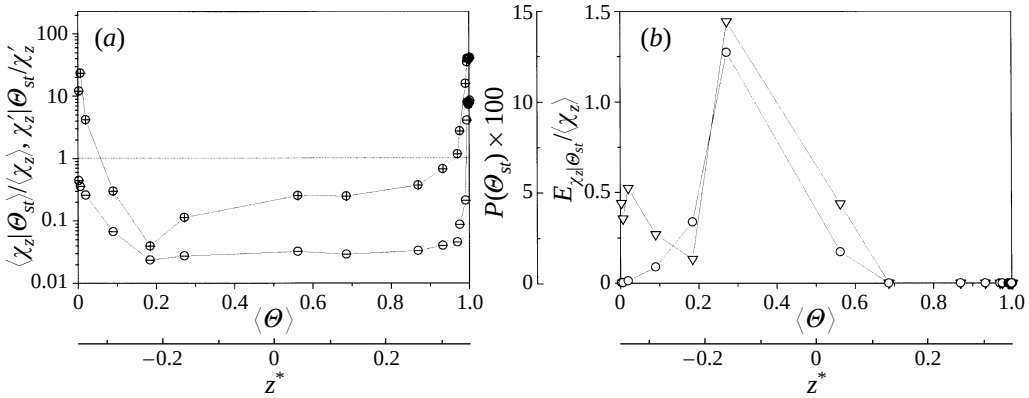

FIGURE 14. (*a*) Centreline distribution of the mean and the r.m.s. of the axial component of the scalar dissipation conditional on $\Theta_{st} = 0.055$. (*b*) Weighted probability $E_{\chi_z|\Theta_{st}}$ and the probability $P(\Theta_{st} = 0.055)$: $\oplus$ mean conditional dissipation; $\ominus$, r.m.s. conditional dissipation; $\triangledown$, weighted probability; $\bigcirc$, scalar probability.

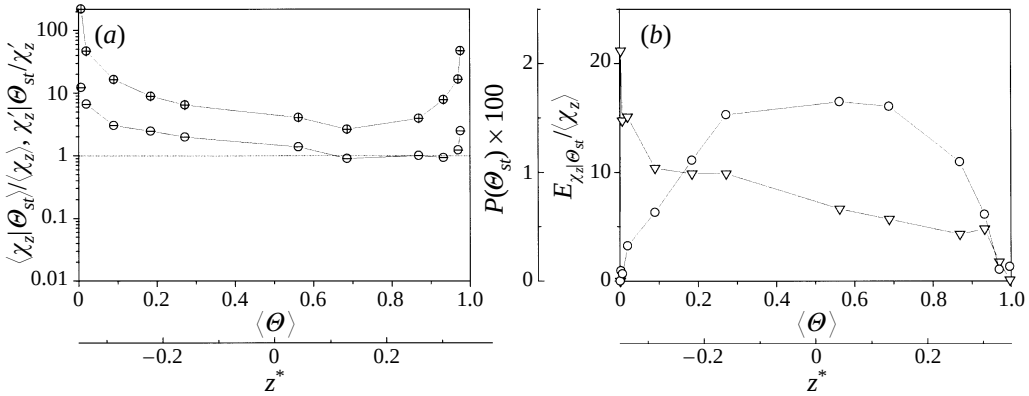

FIGURE 15. As figure 14 but for $\Theta_{st} = 0.3$.

of a methane flame, with the scalar fluctuations and the scalar dissipation assumed statistically independent, would lead to an overestimation of the values of the scalar dissipation at the stoichiometric contour and hence to underestimation of the flame extinction limits, while it will be the opposite for a CO/H_2 flame. This difference between the conditional and the unconditional values is also likely to be valid in the vicinity of the exit of a turbulent jet, which is the stabilization region of a diffusion flame, since it was demonstrated above that the distributions of the mean and r.m.s. conditional dissipation are directly related to, and may be qualitatively predicted by, the shape of the scalar p.d.f. The p.d.f. in this flow is likely to be similar to that of the counterflow mixing layer, which is skewed towards the two streams and bimodal at the scalar interface for residence times smaller than the eddy turn-over and this is supported by the measurements of Stapountzis *et al.* (1986) in a non-combusting flow and by the theoretical approach of Bilger (1980) in a turbulent diffusion flame.

4. Conclusions

Simultaneous values of a passive scalar and of the axial and radial components of the scalar dissipation have been measured for two Reynolds numbers by pairs of

parallel cold wires along the centreline of a counterflow, where one jet was slightly heated. The probability distribution of the scalar fluctuations was bimodal at the stagnation plane, consistent with the fact that the scalar turbulence was 'young', in the sense that the residence times in the mixing layer were short in comparison to the eddy turn-over time, as is the case in the vicinity of the exit of a turbulent jet. Thus the results presented here are likely to be representative of scalar turbulence when mixing first takes place between two streams, for example in the stabilization region of turbulent diffusion flames in practical combustors.

It was found that the scalar fluctuations and their dissipation were strongly correlated within the mixing layer between the two opposing jets. At the boundaries of the mixing layer, where the stoichiometric value of most fuels is located, the correlation coefficient was approximately unity, resulting from the simultaneous occurrence of the largest values of the dissipation and the largest values of the scalar fluctuations. At the stagnation plane, the correlation coefficient was as high as -0.5 and the largest values of the scalar dissipation were associated with small values of the scalar fluctuations. Dependence of the distributions of the mean and r.m.s conditional scalar dissipation on the shape of the scalar p.d.f. was demonstrated by relating the largest dissipation values to the rarest scalar fluctuations and it was found that this dependence was also valid in other flows where scalar dissipation has been measured. The assumption of statistical independence between the scalar fluctuations and their dissipation, commonly introduced in the modelling of turbulent diffusion flames, was not tenable and the mean scalar dissipation conditional on the stoichiometric mixture fraction was larger than the unconditional mean by up to an order of magnitude at the boundaries of the mixing layer.

The probability distributions of the scalar dissipation components deviated from log-normality at the low dissipation values and these departures were larger for the conditional rather than the unconditional p.d.f.s. However, at the higher values of dissipation, corresponding to cumulative probabilities larger than 50%, the p.d.f.s of the conditional dissipation were to a good approximation log-normal so that the adoption of log-normality for the distribution of the conditional scalar dissipation in the context of combustion modelling leads to prediction of flame extinction limits to within 15% provided that the mean and the r.m.s. of the scalar dissipation conditional on the stoichiometric mixture fraction are accurately known.

The authors gratefully acknowledge the financial support provided by the European Union through the HCM-Network contract no. CHRX-CT93-0389.

REFERENCES

Anselmet, F. & Antonia, R. A. 1985 Joint statistics between temperature and its dissipation. *Phys. Fluids* **28**, 1048.

Anselmet, F., Djeridi, H. & Fulachier, L. 1994 Joint statistics of a passive scalar and its dissipation in a turbulent flow. *J. Fluid Mech.* **280**, 173.

Antonia, R. A. & Browne, L. W. B. 1986 Anisotropy of the temperature dissipation on a turbulent wake. *J. Fluid Mech.* **163**, 393.

Antonia, R. A. & Mi, J. 1993 Temperature dissipation in a turbulent round jet. *J. Fluid Mech.* **250**, 531.

Antonia, R. A. & Sreenivasan, K. R. 1977 Skewness of temperature derivatives in turbulent shear flows. *Phys. Fluids* **20**, 1986.

Antonia, R. A. & Van Atta, C. W. 1975 On the correlation between temperature and velocity dissipation fields in a heated turbulent jet. *J. Fluid Mech.* **67**, 273.

Ashurst, W. T., Kerstein, A. R., Kerr, R. M. & Gibson, C. H. 1987 Alignment of vorticity and scalar gradient with strain rate in simulated Navier–Stokes turbulence. *Phys. Fluids* **30**, 2343.

Bilger, R. W. 1980 Turbulent flames with non-premixed reactants. In *Turbulent Reacting Flows* (ed. P. A. Libby & F. A. Williams), p. 65. Springer.

Bilger, R. W. 1988 The structure of turbulent nonpremixed flames In *Twenty-second Symposium* (*Intl*) *on Combustion* p. 475. The Combustion Institute, Pittsburgh.

Bray, K. N. C., Champion, M. & Libby, P. A. 1991 Premixed flames in stagnating turbulence: Part I. The general formulation for counterflow streams and models for gradient transport. *Combust. Flame* **84**, 391.

Bray, K. N. C., Champion, M. & Libby, P. A. 1994 Flames in stagnating turbulence. In *Turbulent Reacting Flows* (ed. P. A. Libby & F. A. Williams), p. 573. Academic.

Champion, M. & Libby, P. A. 1990 Stagnation streamline turbulence revisited. *AIAA J.* **28**, 1525.

Cho, P., Law, C. K., Cheng, R. K. & Shepherd, I. G. 1988 Velocity and scalar fields of turbulent premixed flames in a stagnation flow. In *Twenty-second Symposium* (*Intl*) *on Combustion*, p. 739. The Combustion Institute, Pittsburgh.

Collis, D. C. & Williams, M. J. 1959 Two dimensional convection from heated wires at low Reynolds number. *J. Fluid Mech.* **6**, 357.

Eswaran, V. & Pope, S. B. 1988 Direct numerical simulations of the turbulent mixing of a passive scalar. *Phys. Fluids* **31**, 506.

Everest, D. A., Driscoll, J. F., Dahm, W. J. A. & Feikema, D. A. 1995 Images of two-dimensional field and temperature gradients to quantify mixing rates within a non-premixed turbulent jet flame. *Combust. Flame* **101**, 58.

Gao, F. 1991 Mapping closure and non-Gaussianity of the scalar probability density functions in isotropic turbulence. *Phys. Fluids* A **3**, 2438.

Girimmett, G. R. & Stirzaker, D. R. 1992 *Probability and Random Processes.* Clarendon.

Haworth, D. C., Drake, M. C. & Blint, R. J. 1988 Stretched laminar flamelet modelling of a turbulent jet diffusion flame. *Combust. Sci. Tech.* **60**, 287.

Janicka, J. & Peters, N. 1982 Prediction of turbulent jet diffusion flame lift-off using a pdf transport equation. In *Nineteenth Symposium* (*Intl*) *on Combustion*, p. 367. The Combustion Institute, Pittsburgh.

Jayesh & Warhaft, Z. 1992 Probability distribution, conditional dissipation and transport of passive temperature fluctuations in grid generated turbulence. *Phys. Fluids* A **4**, 2292.

Kailasnath, P., Sreenivasan, K. R. & Saylor, J. R. 1993 Conditional scalar dissipation rates in turbulent wakes, jets and boundary layers. *Phys. Fluids* A **5**, 3207.

Kerstein, A. R. & Ashurst, W. T. 1984 Log-normality of gradients of diffusive scalars in homogeneous, two-dimensional mixing systems. *Phys. Fluids* **27**, 2819.

Kolmogorov, A. N. 1962 A refinement of previous hypothesis concerning the local structure of turbulence in a viscous incompressible fluid at high Reynolds number. *J. Fluid Mech.* **13**, 82.

Kostiuk, L. W. 1991 Premixed turbulent combustion in counterflowing streams. PhD thesis, University of Cambridge.

Kostiuk, L. W., Bray, K. N. C. & Cheng, P. K. 1989 Premixed turbulent combustion in counterflowing streams. *Combust. Sci. Tech.* **64**, 233.

Krishnamoorthy, L. V. & Antonia, R. A. 1987 Temperature-dissipation measurements in a turbulent boundary layer. *J. Fluid Mech.* **176**, 265.

Lee, Y. Y. & Pope, S. B. 1995 Nonpremixed turbulent reacting flow near extinction. *Combust. Flame* **101**, 501.

Liew, S. K., Bray, K. N. C. & Moss, J. B. 1984 A stretched laminar flamelet model of turbulent non-premixed combustion. *Combust. Flame* **56**, 199.

Mastorakos, E., Taylor, A. M. K. P. & Whitelaw, J. H. 1992 Extinction and temperature characteristics of turbulent counterflow flames with partial premixing. *Combust. Flame* **91**, 40.

Mastorakos, E., Taylor, A. M. K. P. & Whitelaw, J. H. 1993 Mixing in turbulent opposed jet flows. In *Turbulent Shear Flows 9* (ed. L. J. S. Bradberry, F. Durst, B. E. Launder, F. W. Schmidt & J. H. Whitelaw), p. 147. Springer.

Mi, J., Antonia, R. A. & Anselmet, F. 1995 Joint statistics between temperature and its dissipation rate components in a round jet. *Phys. Fluids* A **7**, 1665.

Namazian, M., Scheffer, R. W. & Kelly, J. 1988 Scalar dissipation measurements in the developing region of a jet. *Combust. Flame* **74**, 147.

PARATHOEN, P., PETIT, C. & LECORDIER, J. C. 1982 The effect of thermal prong- wire interaction on the response of a cold wire in gaseous flows (air, argon and helium). *J. Fluid Mech.* **124**, 457.

PETERS, N. 1983 Local turbulent quenching due to flame stretch and non-premixed turbulent combustion. *Combust. Sci. Tech.* **30**, 1.

PETERS, N. 1984 Laminar diffusion flamelet models in non-premixed turbulent combustion. *Prog. Energy Combust. Sci.* **10**, 319.

PRASAD, R. R. & SREENIVASAN, K. R. 1990 Quantitative three-dimensional imaging ang the structure of passive scalar fields in fully turbulent flows *J. Fluid Mech.* **216**, 1.

SAHAY, A. & O'BRIEN, E. E. 1993 Uniform mean scalar gradient in grid turbulence: Conditioned dissipation and production. *Phys. Fluids* A **5**, 1076.

SARDI, K. 1997 Turbulent flame extinction in unforced and periodically forced counterflow. PhD thesis, University of London.

SARDI, K., TAYLOR, A. M. K. P. & WHITELAW, J. H. 1996 Experimental investigation of the interaction between scalar dissipation and strain rate in a counterflow geometry. In *The Proceedings Volume of the IUTAM Symposium on Variable Density Low Speed Flows* (ed. L. Fulachier, J. L. Lumley & F. Anselmet). Kluwer.

SREENIVASAN, K. R., ANTONIA, R. A. & DAHN, H. Q. 1977 Temperature dissipation fluctuations in a turbulent boundary layer. *Phys. Fluids* **20**, 1238.

SREENIVASAN, K. R. & TAVOULARIS, S. 1980 On the skewness of the temperature derivative in turbulent flows. *J. Fluid Mech.* **101**, 783.

STAPOUNTZIS, H., SAWFORD, B. L., HUNT, J. C. R. & BRITTER, R. E. 1986 Structure of the temperature field downwind of a line source in grid turbulence. *J. Fluid Mech.* **165**, 401.

STARNER, S. H., BILGER, R. W., LYONS, K. M., FRANK, J. H. & LONG, M. B. 1994 Conserved scalar measurements in turbulent diffusion flames by a Raman and Rayleigh Ribbon Imaging method. *Combust. Flame* **99**, 347.

TAVOULARIS, S. & CORRSIN, S. 1981 Experiments in nearly homogeneous turbulent shear flow with a uniform mean temperature gradient. Part 2. The fine structure. *J. Fluid Mech.* **104**, 349.

TENNEKES, H. & LUMLEY, J. L. 1972 *First Course in Turbulence*. MIT Press.

TSUJI, T., NAGANO, Y. & TAGAWA, M. 1992 Frequency response and instantaneous temperature profile of cold-wire sensors for fluid temperature fluctuation measurements. *Exps. Fluids* **13**, 171.

WYNGAARD, J. C. 1971*a* Spatial resolution of a resistance wire temperature sensor. *Phys. Fluids* **4**, 2052.

WYNGAARD, J. C. 1971*b* The effect of velocity sensitivity on temperature derivative statistics in isotropic turbulence. *J. Fluid Mech.* **48**, 763.